

Electronic Supplementary Material (ESI) for Green Chemistry.

This journal is © The Royal Society of Chemistry 2020

Electronic Supplementary Information

Photocatalytic Carbon Dioxide Reduction Coupled with Benzylamine Oxidation over Zn-Bi₂WO₆ Microflowers

Dongxing Tan,^{a,b} Xiuyan Cheng,^{a,b} Jianling Zhang,^{a,b,c*} Yufei Sha,^{a,b} Xiaojun Shen,^{a,b} Zhuizhui Su,^{a,b} Buxing Han^{a,b,c} and Lirong Zheng^d

^aBeijing National Laboratory for Molecular Sciences, CAS Key Laboratory of Colloid, Interface and Chemical Thermodynamics, CAS Research/Education Center for Excellence in Molecular Sciences, Institute of Chemistry, Chinese Academy of Sciences, Beijing 100190, P.R.China. E-mail: zhangjl@iccas.ac.cn.

^bSchool of Chemical Sciences, University of Chinese Academy of Sciences, Beijing 100190, P.R.China.

^cPhysical Science Laboratory, Huairou National Comprehensive Science Center, Beijing 100190, P.R.China.

^dBeijing Synchrotron Radiation Facility (BSRF), Institute of High Energy Physics, Chinese Academy of Sciences, Beijing 100049, P.R.China.

*Correspondence Email: zhangjl@iccas.ac.cn.

Experimental details

Materials. CO₂ (>99.999% purity) was provided by Beijing Analysis Instrument Factory. Sodium sulfate anhydrous, 4-Methylbenzylamine, 4-chlorobenzylamine, 4-methoxybenzylamine, benzylamine and 4-(trifluoromethyl)benzylamine were purchased from Beijing InnoChem Science & Technology Co., Ltd. Bismuth nitrate pentahydrate and sodium tungstate dihydrate were purchased from J&K Scientific Co., Ltd. Acetonitrile and ethanol were provided by Beijing Chemical Works. Zinc nitrate hexahydrate was provided by Sinopharm Chemical Reagent Beijing Co., Ltd.

Preparation of Zn-Bi₂WO₆ and Bi₂WO₆. In a typical synthesis process of Zn-Bi₂WO₆, bismuth nitrate pentahydrate (1 mmol), and sodium tungstate dihydrate (0.5 mmol) were dispersed in 35 mL of deionized water and stirred at room temperature for 5 min. The appropriate amounts of zinc nitrate hexahydrate was added to the solution and further stirred for 30 min. The mixed solution was transferred into a teflon liner stainless-steel autoclave, which was sealed and heated at 140 °C for 24 h. After the autoclave was cooled down to room temperature, the solid was washed with deionized water and dried in a vacuum oven at 80 °C for 24 h. The synthesis process of Bi₂WO₆ is similar to that of the Zn-Bi₂WO₆, except that zinc nitrate hexahydrate was not added.

Characterizations. The morphologies of the catalysts were characterized by scanning electron microscopy (SEM) (HITACHI S-4800). Transmission electron microscopy (TEM) images were taken on JEOL JEM-EM-1011 and JEOL JEM-2100F field-emission high-resolution transmission electron microscope operated at 200 kV. Atomic force microscopy (AFM) was taken on MultiMode 8. Powder X-ray diffraction (XRD) patterns were conducted on a Rigaku D/max 2400 diffractometer with Cu K α radiation (λ = 0.15418 nm) at a scanning rate of 4° min⁻¹. X-ray photoelectron spectrum (XPS) was carried out with a multipurpose X-ray photoemission spectroscope (Thermo Scientific ESCALAB 250Xi). The element content of Zn was determined by inductively coupled plasma-mass spectrometry. The UV-vis absorption spectra were recorded on a UV-2600 spectrometer and BaSO₄ was used as reference material. The transient state photoluminescence (PL) spectroscopy and steady-state PL spectra were measured using an FLS980 spectrophotometer at room temperature with a 325 nm Xe laser as the excitation light source. The electrochemical impedance spectra and transient photocurrent spectra were measured on a CHI 660D electrochemical station in a 0.5 M Na₂SO₄ solution under ambient conditions. The CO₂ adsorption isotherms were measured at 273K by Autosorb-1-C Quantachrome analyzer. CO₂ temperature-programmed desorption profiles (TPD) spectra were recorded on a catalyst analyzer (AutoChem II 2920). The X-ray absorption fine structure spectroscopy (XAFS) experiment was carried out at Beamline 1W1B at Beijing Synchrotron Radiation Facility. Data of XAFS were processed using the Athena and Artemis programs of the IFEFFIT package based on FEFF 6. Data were processed with k^3 -weighting and a Rbkg value of 1.0. Normalized X-ray absorption near-edge structure (XANES) data were obtained directly from the Athena program of the IFEFFIT package.

Electrochemical test. The electrochemical measurement was implemented in a three-electrode system at electrochemical workstation (CHI660E, Chenhua Instrument, Shanghai, China) with the photocatalyst-coated indium-tin oxide (ITO) as the working electrode, an Ag/AgCl with 3.5 M KCl as a reference electrode and Pt net (1×1 cm) as the counter electrode. The illumination source adopted in photocurrent ON/OFF cycles was a 300 W Xe lamp with full spectrum. A 0.5 M Na₂SO₄ solution (pH = 6.8) was applied as electrolyte. To prepare the catalyst ink, 3 mg of the photocatalyst and 10 μ L of 5 % Nafion 117 solution, as conducting binder, were introduced into 200 μ L of ethanol and sonicated for 1 h. Then the catalyst ink was dropped on the surface of an ITO plate (1×1 cm) to prepare the working electrodes. Mott-Schottky measurements, transient photocurrent spectra and electrochemical impedance spectra were performed in a 0.5 M Na₂SO₄ solution. All the potentials were recorded versus Ag/AgCl (vs. Ag/AgCl) electrode.

Coupling CO₂ reduction and benzylamine oxidation and product analysis. The CO₂ photoreduction and benzylamine oxidation experiment was performed in a 100 mL gas-tight reactor. In a typical process, 5 mg of photocatalyst and 100 μ L of benzylamine were dispersed in 10 mL of acetonitrile. Then, CO₂ (1 atm) was charged into the reactor, which was placed in a water bath of 25 °C. A 300 W Xe lamp was used as simulated sunlight source to start the photoreaction. After reaction for a certain time, the gaseous product was analyzed by a gas chromatograph (HP 7890B) equipped with thermal conductivity detector and flame ionization detector detectors using helium as the internal standard. The liquid was analyzed by ¹H nuclear

magnetic resonance spectroscopy (AVANCE III HD 400 MHz) in methyl sulfoxide- d_6 with tetramethylsilane as the internal standard. For the stability test, the catalyst after photocatalytic reaction was centrifugally separated and vacuum-dried. Then, the next photocatalytic reaction was carried out with the recovered catalyst.

Apparent quantum efficiency. The apparent quantum efficiency (QE) for Zn-Bi₂WO₆ was tested under the same photocatalytic reaction condition except for the light source. One Xe lamp (300 W, 280 nm), positioned 100 mm away from the reactor, was used as light source to trigger the photocatalytic reaction. The average intensity of irradiation was evaluated by the light intensity and the irradiation area. The QE of CO generation was calculated to be 1.89% from the following equation.

$$\phi = \frac{2 \times \text{amount of CO molecules evolved}}{\text{number of incident photons}} \times 100\%$$

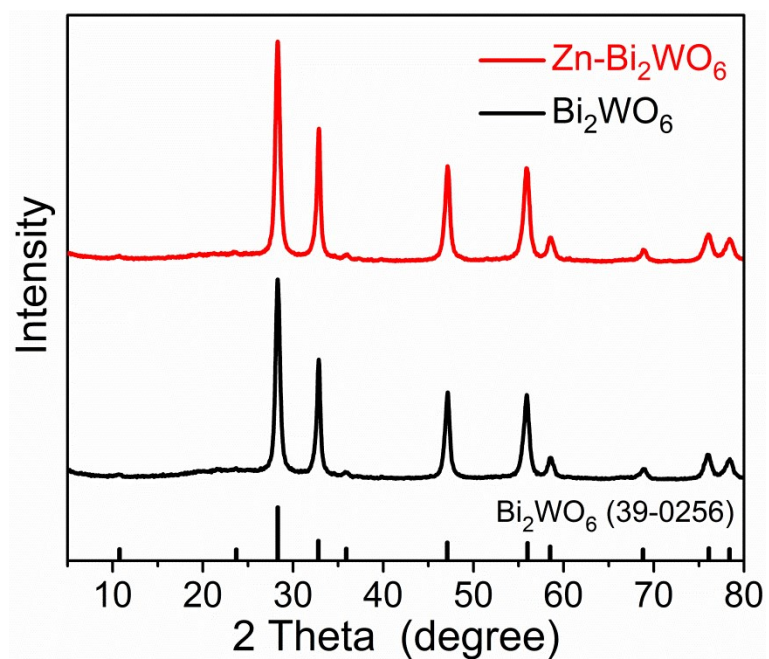


Fig.S1 XRD patterns of Zn-Bi₂WO₆ and Bi₂WO₆. The standard diffraction pattern for Bi₂WO₆ (JCPDS no. 39-0256) is provided as references.

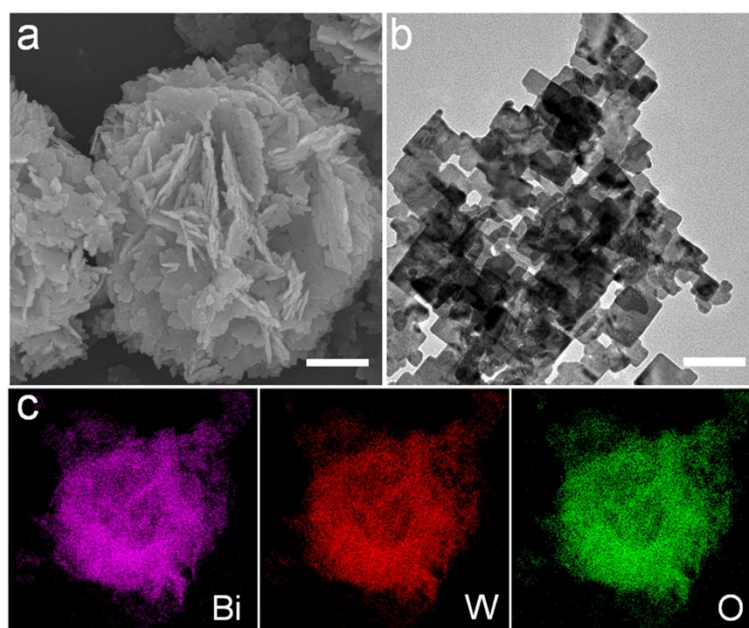


Fig. S2 (a) SEM image, (b) TEM image and (c) EDX mappings of Bi₂WO₆. Scale bars: 500 nm (a), 100 nm (b).

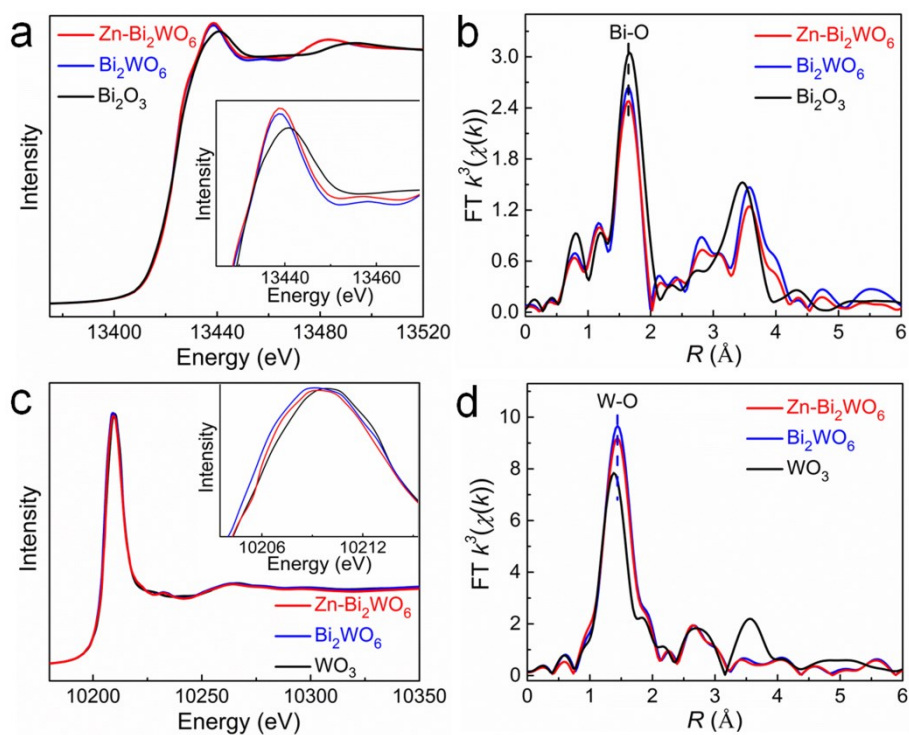


Fig. S3 (a) Bi L₃-edge XANES spectra and (b) fourier transform of Bi L₃-edge EXAFS spectra of Zn-Bi₂WO₆ and Bi₂WO₆. Bi₂O₃ foil was used as contrast sample. (c) W L₃-edge XANES spectra and (d) fourier transform of W L₃-edge EXAFS spectra of Zn-Bi₂WO₆ and Bi₂WO₆. WO₃ was used as contrast sample.

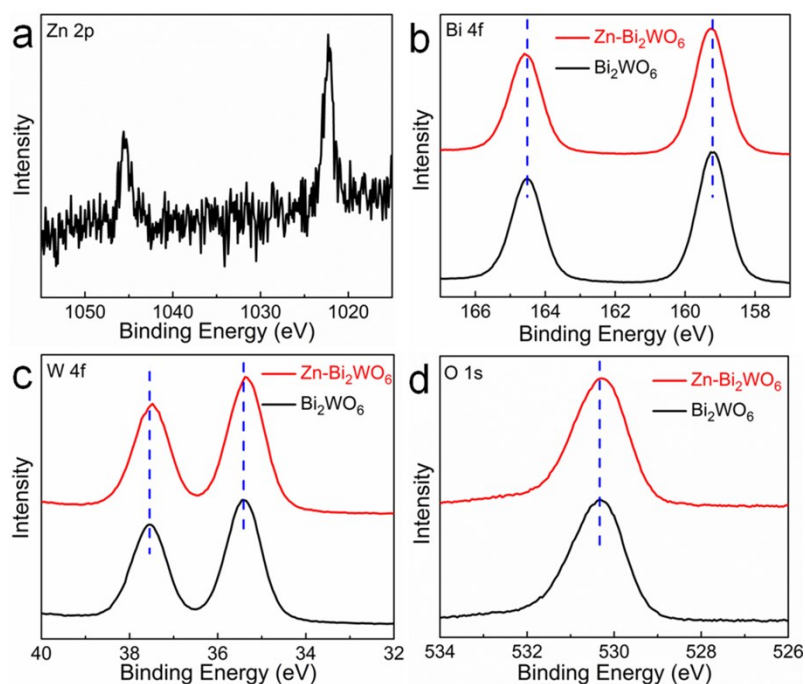


Fig. S4 (a) High-resolution XPS spectrum of Zn 2p of Zn-Bi₂WO₆. High-resolution XPS spectra of (b) Bi 4f, (c) W 4f and (d) O 1s of Zn-Bi₂WO₆ and Bi₂WO₆. For the high-resolution XPS spectra of Zn 2p, the binding energies at 1022.42 and 1045.73 eV are assigned to Zn 2p_{3/2} and Zn 2p_{1/2} of Zn²⁺, respectively. For the high-resolution XPS spectra of Bi 4f, Zn-Bi₂WO₆ shows the binding energies at 159.25 and 164.58 eV corresponding to Bi 4f_{5/2} and Bi 4f_{7/2}, while Bi₂WO₆ shows the binding energies at 159.23 and 164.54 eV, respectively. For the high-resolution XPS spectra of W 4f, Zn-Bi₂WO₆ shows the binding energies at 35.36 and 37.49 eV corresponding to W 4f_{5/2} and W 4f_{7/2}, while Bi₂WO₆ shows the binding energies at 35.40 and 37.55 eV, respectively. For the high-resolution XPS spectra of O 1s, Zn-Bi₂WO₆ shows the binding energy at 530.28 eV corresponding to O-metal, while Bi₂WO₆ shows the binding energy at 530.33 eV. These changes indicate the chemical environmental change of Bi₂WO₆ with Zn²⁺ doping.

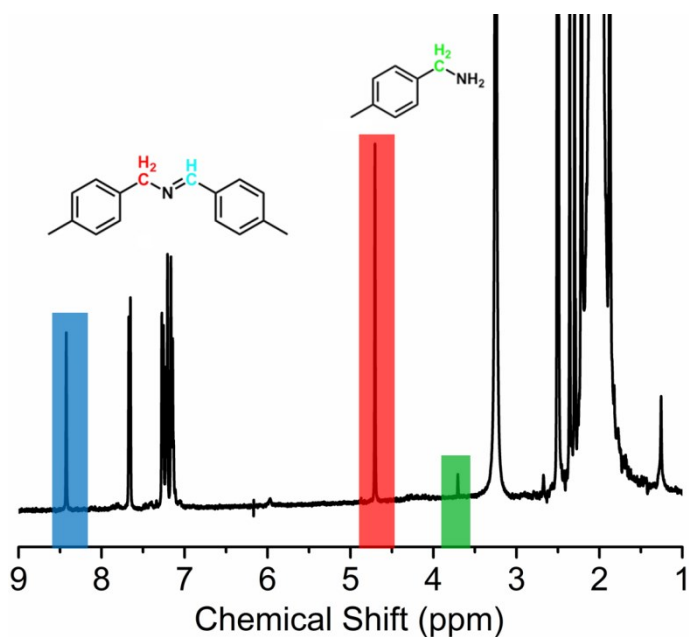


Fig. S5 ¹H nuclear magnetic resonance spectrum of the reaction mixture after photocatalytic CO₂RR and 4-methylbenzylamine oxidation reaction.

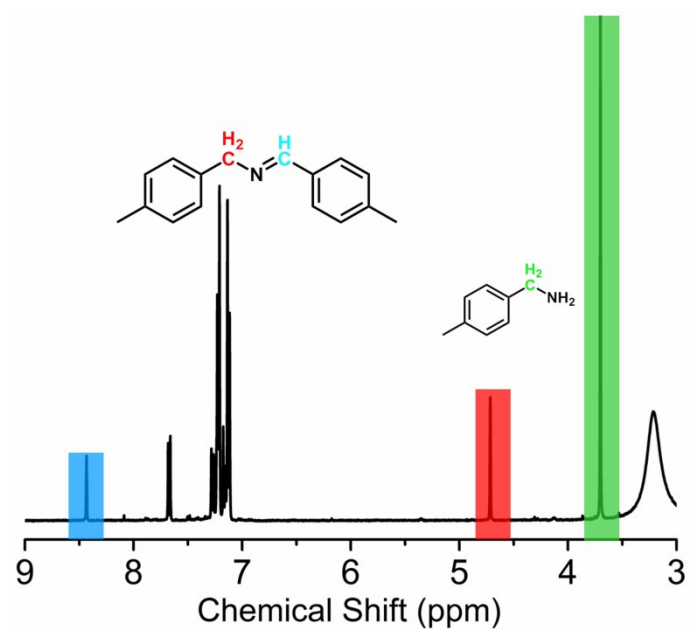


Fig. S6 ^1H nuclear magnetic resonance spectrum of the reaction mixture after photocatalytic 4-methylbenzylamine oxidation reaction in air.

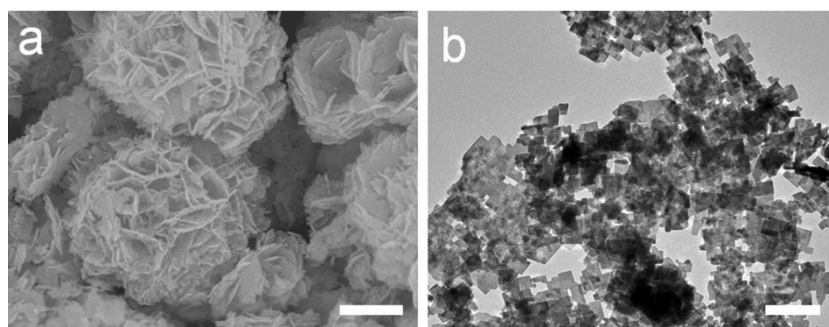


Fig. S7 (a) SEM image and (b) TEM image of $\text{Zn-Bi}_2\text{WO}_6$ after photocatalytic reaction. Scale bars, 1 μm (a) and 200 nm (b).

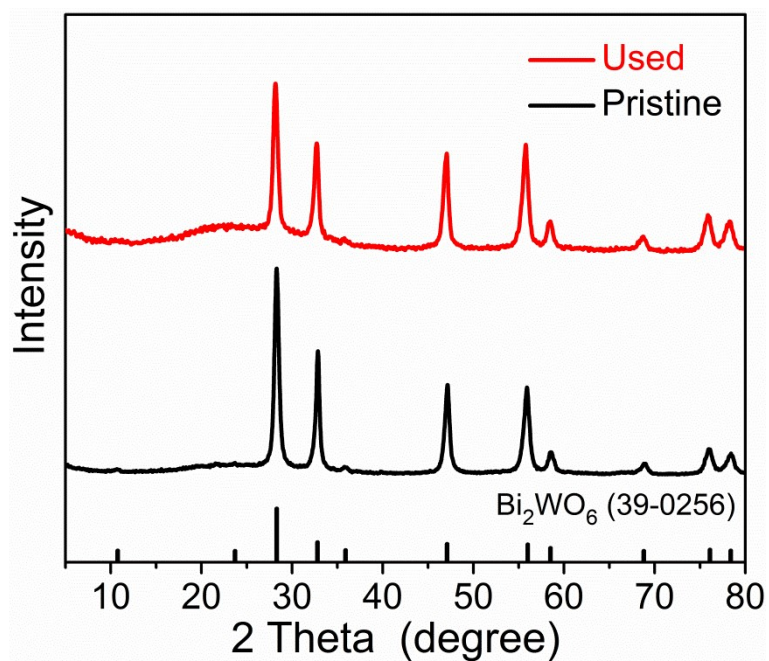


Fig. S8 XRD patterns of Zn-Bi₂WO₆ before and after photocatalytic reaction. The standard diffraction pattern for Bi₂WO₆ (JCPDS no. 39-0256) is provided as references.

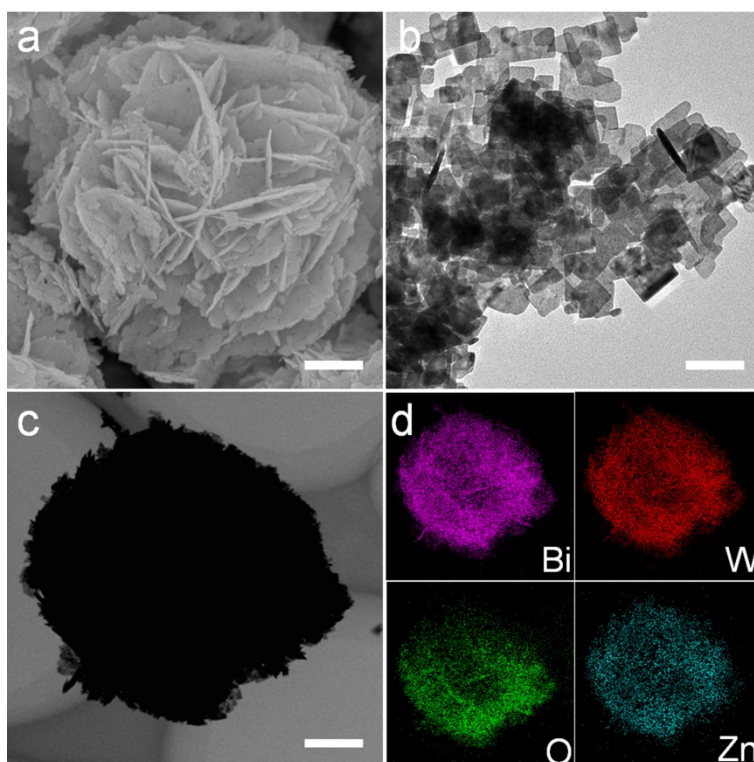


Fig. S9 SEM (a) SEM image, (b) TEM image and (c, d) EDX mappings of Zn-Bi₂WO₆ with Zn content of 0.4 wt%. Scale bars, 500 nm (a), 100 nm (b) and 500 nm (c).

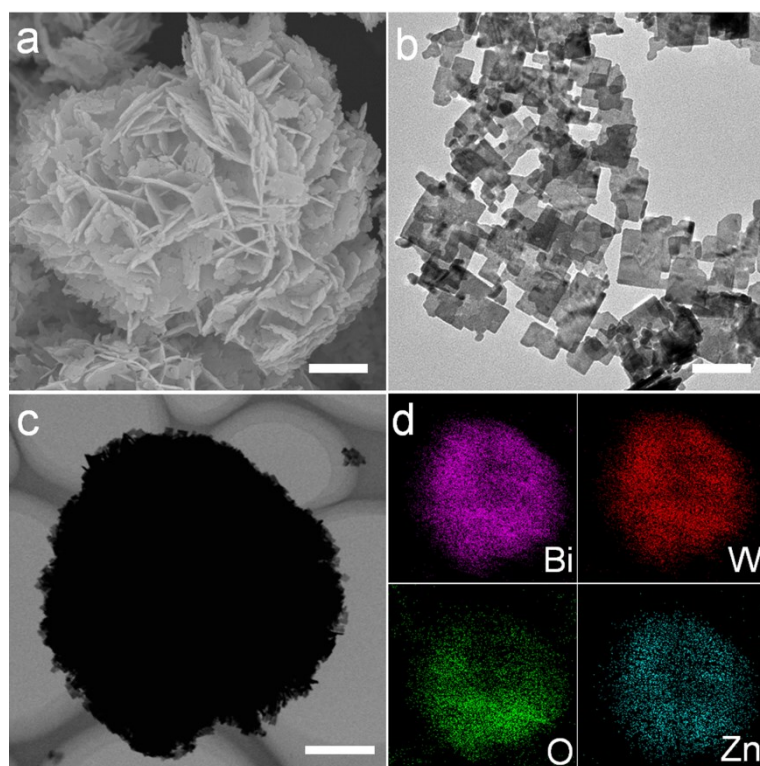


Fig. S10 (a) SEM image, (b) TEM image and (c, d) EDX mappings of $\text{Zn-Bi}_2\text{WO}_6$ with Zn content of 1.8 wt%. Scale bars, 500 nm (a), 100 nm (b) and 500 nm (c).

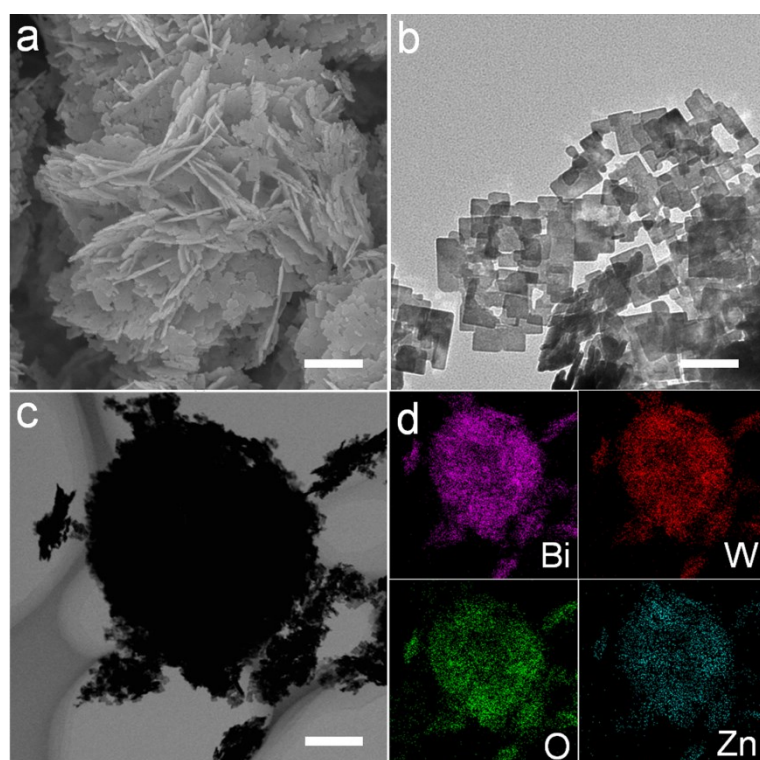


Fig. S11 (a) SEM image, (b) TEM image and (c, d) EDX mappings of $\text{Zn-Bi}_2\text{WO}_6$ with Zn content of 2.3 wt%. Scale bars, 500 nm (a), 100 nm (b), 500 nm (c).

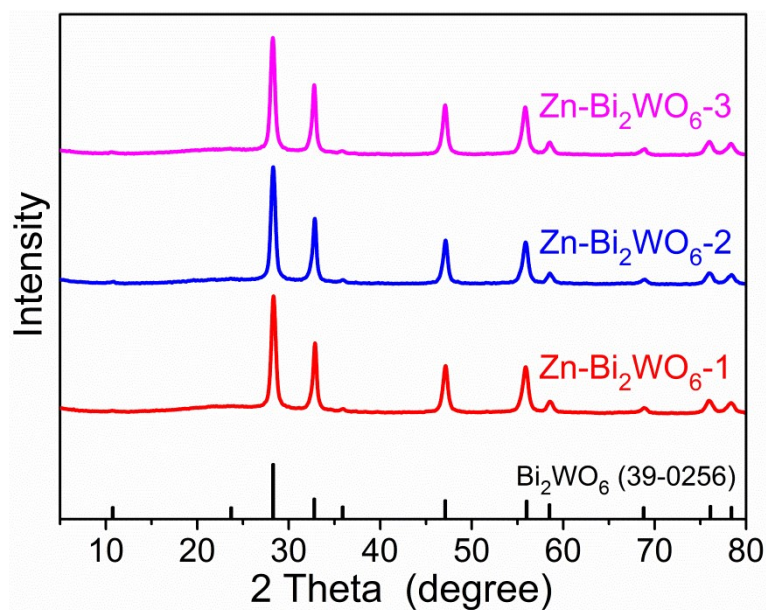


Fig. S12 XRD patterns of Zn-Bi₂WO₆ with Zn content of 0.4 wt% (Zn-Bi₂WO₆-1), 1.8 wt% (Zn-Bi₂WO₆-2) and 2.3 wt% (Zn-Bi₂WO₆-3). The standard diffraction pattern for Bi₂WO₆ (JCPDS no. 39-0256) is provided as reference.

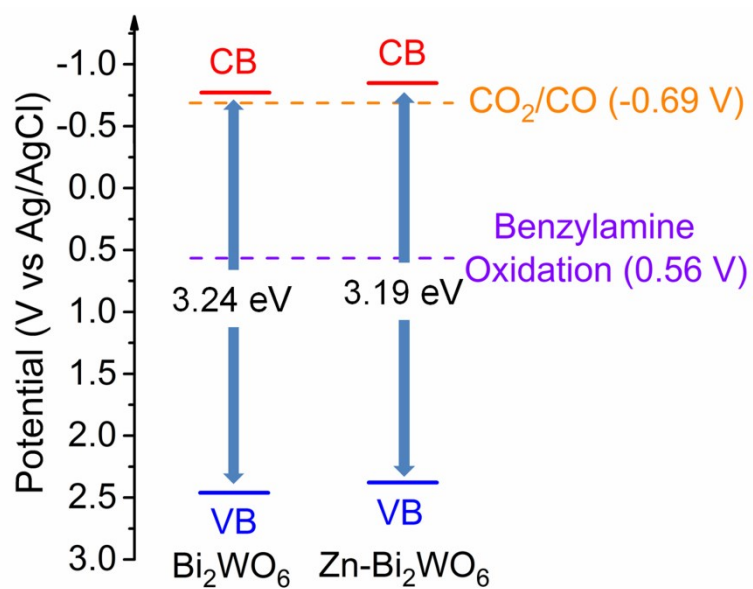


Fig. S13 Band structures of Zn-Bi₂WO₆ and Bi₂WO₆.

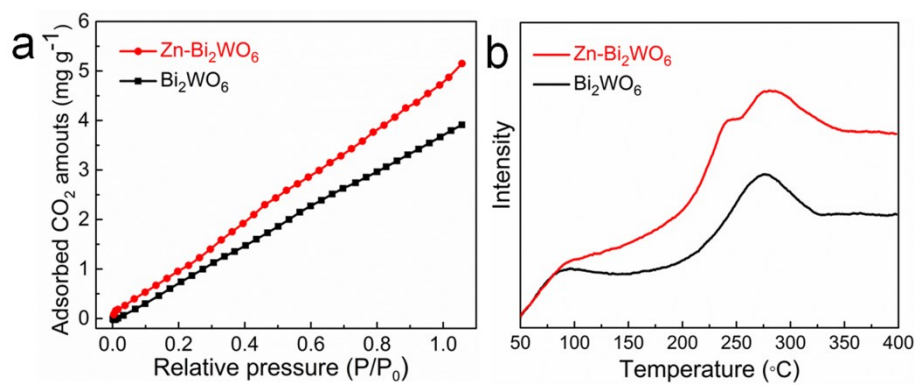


Fig. S14 (a) CO₂ adsorption isotherms at 273 K and 1 atm and (b) CO₂ temperature-programmed desorption profiles for Zn-Bi₂WO₆ and Bi₂WO₆.

Table S1. Comparison of the activities of Zn-Bi₂WO₆ photocatalyst with the reported photocatalysts for CO₂ reduction to CO.

Photocatalysts	Light sources	Reaction conditions	Products	Efficiencies (μmol g ⁻¹ h ⁻¹)	Ref.
Zn-Bi ₂ WO ₆	Xe lamp	Liquid-solid	CO	127.5	This work
Defect-rich Bi ₁₂ O ₁₇ Cl ₂ nanotube	Xe lamp	Liquid-solid	CO	48.6	1
One-unit-cell ZnIn ₂ S ₄	Xe lamp	Liquid-solid	CO	33.2	2
Oxygen-defect BiOBr atomic layers	Xe lamp	Liquid-solid	CO	87.4	3
Oxygen-rich WO ₃ layers	IR light	Liquid-solid	CO	2.8	4
Co-Bi ₃ O ₄ Br-1	Xe lamp	Liquid-solid	CO	107.1	5
BiOCl with oxygen vacancies	Xe lamp	Liquid-solid	CO	1.01	6
Bi ₄ O ₅ BrI	Xe lamp	Liquid-solid	CO	22.8	7
V _{Bi} -BiOBr ultrathin nanosheets	Xe lamp	Liquid-solid	CO	20.1	8
TTCOF-Zn	Xe lamp	Liquid-solid	CO	12.3	9
CsPbBr ₃ QD/GO	Xe lamp	Liquid-solid	CO, CH ₄	58.7, 29.6	10
Partially oxidized SnS ₂ atomic layers	Xe lamp	Gas-solid	CO	12.3	11
α-Fe ₂ O ₃ /g-C ₃ N ₄	Xe lamp	Gas-solid	CO	27.2	12
PEosinY-1	Xe lamp	Gas-solid	CO	33.0	13
CdS/N-doped graphene	Xe lamp	Gas-solid	CO, CH ₄	2.6, 0.3	14
Layered Zinc Silicate Nanosheets	Xe lamp	Gas-solid	CO	126.7	15
BON-Br	Xe lamp	Gas-solid	CO	8.12	16
QS-Co ₃ O ₄ HoMSs (ZIF-67)	Xe lamp	Gas-solid	CO	46.13	17
Single-Crystalline InVO ₄ Sheets	Xe lamp	Gas-solid	CO, CH ₄	18.3, 0.3	18
HCP-TiO ₂ -FG	Xe lamp	Gas-solid	CO, CH ₄	21.6, 27.6	19
CuS atomic layers	Xe lamp	Gas-solid	CO	14.5	20

Table S2. Comparison of the activities of Zn-Bi₂WO₆ photocatalyst with the reported photocatalysts for 4-Methylbenzylamine oxidation reaction.

Photocatalysts	Light sources	Reaction conditions	Selectivity	Efficiencies (mmol g ⁻¹ h ⁻¹)	Ref.
Zn-Bi ₂ WO ₆	Xe lamp	CO ₂	>99%	13.1	This work
PCN-222	Xe lamp	Air	>99%	10.0	21
ZnIn ₂ S ₄	Xe lamp	Air	96.2%	8.0	22
HNb ₃ O ₈	Xe lamp	Air	92.4%	0.9	23
mesoporous g-C ₃ N ₄	Xe lamp	O ₂	98%	3.7	24
Ordered mesoporous Au/TiO ₂ nanospheres	Halogen tungsten lamp	O ₂	>99%	1.6	25
Cd(dcbpy)	Xe lamp	Air	>99%	2.7	26
C-CMP	Xe lamp	O ₂	95%	5.9	27
CF-HCP	LED lamp	O ₂	/	4.8	28
[Au ₂₅]/TiO ₂	LED lamp	O ₂	>99%	6.7	29
CdS@C ₃ N ₄	LED lamp	Air	>99%	5.3	30

References

- 1 J. Di, C. Zhu, M. Ji, M. Duan, R. Long, C. Yan, K. Gu, J. Xiong, Y. She, J. Xia, H. Li and Z. Liu, *Angew. Chem. Int. Ed.*, 2018, **57**, 14847–14851.
- 2 X. Jiao, Z. Chen, X. Li, Y. Sun, S. Gao, W. Yan, C. Wang, Q. Zhang, Y. Lin and Y. Luo, *J. Am. Chem. Soc.*, 2017, **139**, 7586–7594.
- 3 J. Wu, X. Li, W. Shi, P. Ling, Y. Sun, X. Jiao, S. Gao, L. Liang, J. Xu, W. Yan, C. Wang and Y. Xie, *Angew. Chem. Int. Ed.*, 2018, **57**, 8719–8723.
- 4 L. Liang, X. Li, Y. Sun, Y. Tan, X. Jiao, H. Ju, Z. Qi, J. Zhu and Y. Xie, *Joule*, 2018, **2**, 1–13.
- 5 J. Di, C. Chen, S. Yang, S. Chen, M. Duan, J. Xiong, C. Zhu, R. Long, W. Hao, Z. Chi, H. Chen, Y. Weng, J. Xia, L. Song, S. Li, H. Li and Z. Liu, *Nat. Commun.*, 2019, **10**, 2840.
- 6 L. Zhang, W. Wang, D. Jiang, E. Gao and S. Sun, *Nano Res.*, 2015, **8**, 821–831.
- 7 Y. Bai, L. Ye, T. Chen, P. Wang, L. Wang, X. Shi and P. Wong, *Appl. Catal. B*, 2017, **203**, 633–640.
- 8 J. Di, C. Chen, C. Zhu, P. Song, J. Xiong, M. Ji, J. Zhou, Q. Fu, M. Xu, W. Hao, J. Xia, S. Li, H. Li and Z. Liu, *ACS Appl. Mater. Interfaces*, 2019, **11**, 30786–30792.
- 9 M. Lu, J. Liu, Q. Li, M. Zhang, M. Liu, J. Wang, D. Yuan and Y. Lan, *Angew. Chem. Int. Ed.*, 2019, **58**, 12392–12397.
- 10 Y. Xu, M. Yang, B. Chen, X. Wang, H. Chen, D. Kuang and C. Su, *J. Am. Chem. Soc.*, 2017, **139**, 5660–5663.
- 11 X. Jiao, X. Li, X. Jin, Y. Sun, J. Xu, L. Liang, H. Ju, J. Zhu, Y. Pan, W. Yan, Y. Lin and Y. Xie, *J. Am. Chem. Soc.*, 2017, **139**, 18044–18051.
- 12 Z. Jiang, W. Wan, H. Li, S. Yuan, H. Zhao and P. Wong, *Adv. Mater.*, 2018, **30**, 9.
- 13 X. Yu, Z. Yang, B. Qiu, S. Guo, P. Yang, B. Yu, H. Zhang, Y. Zhao, X. Yang, B. Han and Z. Liu, *Angew. Chem. Int. Ed.*, 2019, **58**, 632–636.
- 14 C. Bie, B. Zhu, F. Xu, L. Zhang and J. Yu, *Adv. Mater.*, 2019, **31**, 1902868.
- 15 L. Wang, D. Bahnemann, L. Bian, G. Dong, J. Zhao and C. Wang, *Angew. Chem. Int. Ed.*, 2019, **58**, 8103–8108.
- 16 L. Hao, L. Kang, H. Huang, L. Ye, K. Han, S. Yang, H. Yu, M. Batmunkh, Y. Zhang and T. Ma, *Adv. Mater.*, 2019, **31**, 7.
- 17 L. Wang, J. Wan, Y. Zhao, N. Yang and D. Wang, *J. Am. Chem. Soc.*, 2019, **141**, 2238–2241.
- 18 Q. Han, X. Bai, Z. Man, H. He, L. Li, J. Hu, A. Alsaedi, T. Hayat, Z. Yu, W. Zhang, J. Wang, Y. Zhou and Z. Zou, *J. Am. Chem. Soc.*, 2019, **141**, 4209–4213.
- 19 S. Wang, M. Xu, T. Peng, C. Zhang, T. Li, I. Hussain, J. Wang and B. Tan, *Nat. Commun.*, 2019, **10**, 676.
- 20 X. Li, L. Liang, Y. Sun, J. Xu, X. Jiao, X. Xu, H. Ju, Y. Pan, J. Zhu and Y. Xie, *J. Am. Chem. Soc.*, 2019, **141**, 423–430.
- 21 C. Xu, H. Liu, D. Li, J. Su and H. Jiang, *Chem. Sci.*, 2018, **9**, 3152–3158.
- 22 L. Ye and Z. Li, *ChemCatChem*, 2014, **6**, 2540–2543.
- 23 J. Chen, H. Wang, Z. Zhang, L. Han, Y. Zhang, F. Gong, K. Xie, L. Xu, W. Song and S. Wu, *J. Mater. Chem. A*, 2019, **7**, 5493–5503.
- 24 F. Su, S. Mathew, L. Mohlmann, M. Antonietti, X. Wang and S. Blechert, *Angew. Chem. Int. Ed.*, 2011, **50**, 657–660.
- 25 J. Yang and C. Mou, *Appl. Catal. B*, 2018, **231**, 283–291.
- 26 J. Shi, J. Zhang, T. Liang, D. Tan, X. Tan, Q. Wan, X. Cheng, B. Zhang, B. Han, L. Liu, F. Zhang and G. Chen, *ACS Appl. Mater. Interfaces*, 2019, **11**, 30953–30958.
- 27 C. Su, X. Duan, J. Miao, Y. Zhong, W. Zhou, S. Wang and Z. Shao, *ACS Catal.*, 2017, **7**, 388–397.
- 28 Y. Zhi, K. Li, H. Xia, M. Xue, Y. Mu and X. Liu, *J. Mater. Chem. A*, 2017, **5**, 8697–8704.
- 29 H. Chen, C. Liu, M. Wang, C. Zhang, N. Luo, Y. Wang, H. Abroshan, G. Li and F. Wang, *ACS Catal.*, 2017, **7**, 3632–3638.
- 30 Y. Xu, Y. Chen and W. Fu, *Appl. Catal. B*, 2018, **236**, 176–183.